Journal of Physics B: Atomic, Molecular and Optical Physics

PAPER

Frequency up/down conversion by multiphoton pumping in superconducting qubit circuits

To cite this article: H Z Jooya *et al* 2020 *J. Phys. B: At. Mol. Opt. Phys.* **53** 155502

IOP Publishing Journal of Physics B: Atomic, Molecular and Optical Physics
J. Phys. B: At. Mol. Opt. Phys. **53** (2020) 155502 (9pp) https://doi.org/10.1088/1361-6455/ab91e4

Frequency up/down conversion by multiphoton pumping in superconducting qubit circuits

H Z Jooya[1,5], G Sun[2,3,5], J Pan[2,3], P Wu[2,3] and S Han[4]

[1] ITAMP, Harvard-Smithsonian Center for Astrophysics, Cambridge, MA 02138, United States of America
[2] Research Institute of Superconductor Electronics, School of Electronic Science and Engineering, Nanjing University, Nanjing 210093, People's Republic of China
[3] The Purple Mountain Laboratories, Nanjing 211111, People's Republic of China
[4] Department of Physics and Astronomy, University of Kansas, Lawrence, KS 66045, United States of America

E-mail: h.z.jooya@gmail.com and gzsun@nju.edu.cn

Received 21 January 2020, revised 28 April 2020
Accepted for publication 11 May 2020
Published 24 June 2020

Abstract

We propose a versatile scheme for multiphoton frequency up/down conversion in flux superconducting qubit circuits, driven by a pair of microwaves tuned near and far off the qubit resonance. Flux qubits can be engineered with strong anharmonicity such that the two lowest eigenstates are energetically well separated from the higher ones. We demonstrate the high order non-linear transitions between the two lowest levels in the three-photon regime, by coupling the qubit to bichromatic microwave fields with the same Rabi frequencies. Both up and down conversions are presented and accurately interpreted with many-mode Floquet formalism. An intuitive graph theoretic approach elucidates the physics of multiphoton pumping and population trapping. The analytical solutions also illustrate how controllability is achievable for desired single- or multiphoton pumping processes in a wide range of frequencies. The proposed design and theoretical approach are applicable in maintaining the inter-connectivity of future superconducting quantum machines.

Keywords: multiphoton pumping, Floquet, frequency conversion, superconducting qubits

(Some figures may appear in colour only in the online journal)

Superconducting (SC) qubits are leading contenders for demonstration of the so-called quantum supermacy [1]. Achieving this task requires scaling up the number of qubits. Since in many SC qubits circuits, microwaves couple the qubits and shuttle information [2], efficient frequency conversion (FC) is important for interconnection among the qubits and for hybrid quantum systems composed of SC qubits as components [3–7]. Variety of schemes have been proposed for FC at microwave frequencies. Microwave down-conversion has been demonstrated for three-level Λ qubits [8] and studied theoretically when a superconducting Cooper-pair box qubit is located inside a transmission line resonator [9]. Microwave up-conversion has been reported for a two-photon driven flux qubit [10]. These conversions have been achieved in circuit quantum electrodynamics systems, in the strong light–matter coupling regime [11]; and each scheme has been specifically proposed for either up- or down-conversion mechanism.

Motivated by the rapidly growing interest in Floquet engineering [4, 12] and the ubiquitous use of microwave drives in quantum information processing [13], we propose a readily attainable scheme of generating broadband bi-directional FC of microwave photons with the use of a single SC flux qubit embedded in a superconducting microwave cavity and driven by bichromatic classical microwaves. The flux qubit consists of a superconducting loop interrupted by one

[5] Authors to whom any correspondence should be addressed.

[14] or three [15] Josephson junctions. We show that both up- and down-conversions can be achieved by multiphoton excitations between a pair of microwave fields that drive the flux SC qubit circuit in three-photon transition regime. Multiphoton processes have recently attracted much attention in the field of superconducting qubits, due to the new possibilities that such nonlinear effects can provide flexible qubit control as well as being of fundamental physical interest [16–18]. In the case of frequency up-conversion being able to use lower frequencies may also substantially simplify microwave engineering and qubit circuit integration [19, 20].

The implemented theoretical formalism is developed within the two-mode Floquet framework. The Floquet quasienergy diagram is equivalent to the fully quantized dressed-atom picture [21]. Dressed superconducting qubits [22], have been theoretically studied [23, 24] and experimentally demonstrated [25–28]. Based on this method, we propose an effective Hamiltonian approach which provides an accurate and lucid representation of various underlying multiphoton dynamics for the distinct quantum interference patterns observed in the three-photon absorption spectrum.

The superconducting flux qubit is a compound Josephson junction (CJJ) rf superconducting quantum interference device (SQUID) [29]. It consists of a main loop and a CJJ loop subjected to external flux biases Φ_x and $\Phi_x^{\rm CJJ}$, respectively. The CJJ loop is interrupted by two nominally identical Josephson tunnel junctions connected in parallel with total capacitance C and critical current $I_{\rm c}$. The CJJ and main loops have inductances $L_{\rm CJJ}$ and L, respectively. For $L_{\rm CJJ} \ll L$, the Hamiltonian of the CJJ rf SQUID can be approximated by that of a simple rf SQUID as,

$$\hat{H} = \frac{Q^2}{2C} + U(\Phi), \tag{1}$$

where Φ is the total flux threading the main loop and Q is the charge stored in the capacitance. The potential energy of the rf SQUID is,

$$U(\Phi) = \frac{(\Phi - \Phi_x)^2}{2L} - E_J \cos\left(\frac{\pi\Phi_x^{\rm CJJ}}{\Phi_0}\right)\cos\left(\frac{2\pi\Phi}{\Phi_0}\right), \tag{2}$$

where $E_J = \Phi_0 I_{\rm c}/2\pi$ and $\Phi_0 \equiv h/2e$ is the flux quantum. For $\beta_L(\Phi_x^{\rm CJJ}) \equiv (2\pi L I_{\rm c}/\Phi_x)\cos(\pi\Phi_x^{\rm CJJ}/\Phi_0) \geqslant 1$, $U(\Phi)$ is a double-well potential and thus this device can be operated as a qubit for $-\Phi_0/2 \leqslant \Phi_x^{\rm CJJ} \leqslant \Phi_0/2$ and $\Phi_x \approx \Phi_0/2$. This has been verified by microwave spectroscopy studies [14] that the flux qubit can be engineered such that the two lowest eigenstates are energetically well separated from the higher ones [30].

Denoting the counterclockwise as the positive direction of the persistent current $I_{\rm p}$ in the loop, the two logic states of the qubit, $|g\rangle$ and $|e\rangle$, correspond to $I_{\rm p} < 0$ and $I_{\rm p} > 0$ and thus the flux particle in the left- and right-hand wells, respectively. The state-dependent persistent current is given by $I_{\rm p} = \langle g|\,(\Phi - \Phi_x)/L\,|g\rangle$ or $I_{\rm p} = \langle e|\,(\Phi - \Phi_x)/L\,|e\rangle$. If the temperature is much less than the small oscillation frequency (i.e., the plasma frequency) at the bottom of the double-well potential the superconducting flux qubit can be described by a 2×2 effective Hamiltonian matrix [25, 31],

$$\hat{H}_q = -\frac{1}{2}(\varepsilon_0\sigma_z + \Delta\sigma_x), \tag{3}$$

where σ_x, σ_z are Pauli matrices and ε_0 is the detuning energy that is proportional to dc flux bias, $\varepsilon_0 = 2|I_{\rm p}|\delta\Phi_x$ where $\delta\Phi_x = \Phi_x - \Phi_0/2$ is the flux detuning. Equation is obtained using the two logic states of the qubit, $|g\rangle = (1 \quad 0)^T$ and $|e\rangle = (0 \quad 1)^T$, as the bases, with energy separation of $E = \pm\sqrt{\varepsilon_0^2 + \Delta^2}/2$. These two states are coupled through the tunneling strength Δ, which is given by the energy separation of two eigenstates of H_0 at ε_0 which are $(|g\rangle - |e\rangle)/\sqrt{2}$ and $(|g\rangle + |e\rangle)/\sqrt{2}$. Both $|I_{\rm p}|$ and Δ are controlled *in situ* by $\Phi_x^{\rm CJJ}$. Note that $I_{\rm p}$ is a decreasing function of $\Phi_x^{\rm CJJ}$, while Δ increases from zero to the plasma frequency as $\Phi_x^{\rm CJJ}$ approaches $\pm\Phi_0/2$. For $\Phi_x^{\rm CJJ} = 0$ one expects $\Delta \to 0$. When the qubit becomes localized in $|g\rangle$ or $|e\rangle$, $I_{\rm p}$ generates a magnetic flux that can be resolved by an inductively coupled dc SQUID [29].

The time-dependent Hamiltonian describing the flux qubit [32, 33] is,

$$\hat{H} = \hat{H}_q + \hat{H}_{\rm int}, \tag{4}$$

where, the interaction between the microwave and the flux qubit is described by longitudinal coupling,

$$\hat{H}_{\rm int} = -\frac{1}{2}\mathcal{E}(t)\sigma_z, \tag{5}$$

where $\mathcal{E}(t)$ represent the interaction of the qubit with a time-dependent magnetic flux. In this work we investigate a flux qubit driven by a bichromatic microwave (Mw) fields with frequencies ω_1 and ω_2 and magnetic flux amplitudes Φ_1 and Φ_2. The corresponding qubit-microwave interaction is described by,

$$\mathcal{E}(t) = \sum_{i=1}^{2} A_i\,\cos(\omega_i t + \varphi_i), \tag{6}$$

where $A_i = I_{\rm p}\Phi_i$ and $I_{\rm p}$ is the persistent current of the flux qubit. For simplicity, we set $\varphi_i = 0$. The effects of the tunnel splitting and the microwave amplitudes on the transition spectrum are evaluated in the appendix A. For the presented results $\varepsilon_0/2\pi$ is set to 8.8356 GHz, the tunnel splitting $\Delta = 8 \times 10^{-3}\varepsilon_0$ and $A_1 = A_2 = 8 \times 10^{-2}\varepsilon_0$. The qubit transition frequency is $\omega_q = \sqrt{\varepsilon_0^2 + \Delta^2} \simeq \varepsilon_0$. Due to such detuning capability of potential energy, the inversion symmetry for these superconducting qubits can be broken and the parity restriction is lifted. Therefore, the selection rules do not apply. As a result, (even- and odd-) multiphoton and single-photon processes can coexist in such artificial systems [34–36]. The Hamiltonian for longitudinal qubit-field coupling, $\hat{H}_{\rm L}$, can be obtained from the transverse form, $\hat{H}_{\rm T}$, under unitary transformation: $\hat{H}_{\rm L} = U^{-1}\hat{H}_{\rm T}U$, where $U = 1/\sqrt{2}\begin{pmatrix} 1 & -1 \\ 1 & 1 \end{pmatrix}$. This implies that both of these schemes can be used to achieve odd-valued multiphoton processes between two adjacent energy levels. The even-valued multiphoton transitions, however, is obtained only

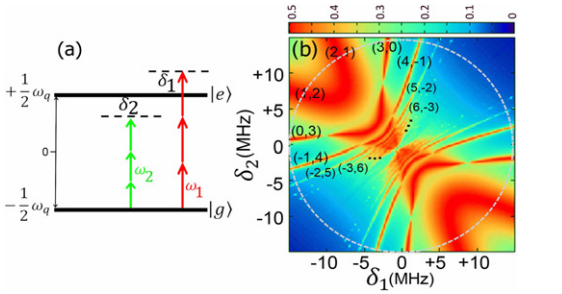

Figure 1. (a) The energy level and microwave drive diagrams represent the three-photon transition in a two-level system. (b) The calculated three-photon transition spectrum. The color map (z-axis) shows the transition probability from $|g\rangle$ to $|e\rangle$. The frequency conversion along the white-dashed circle will be discussed in figure 2(a). The number of photons involved in each transition is labeled accordingly.

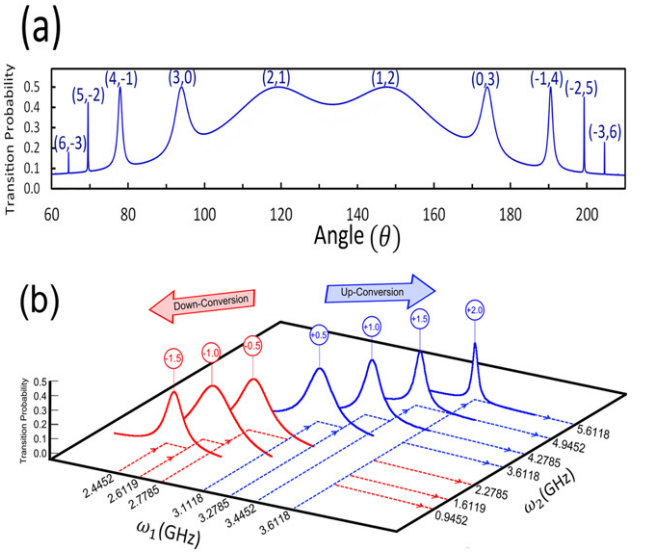

Figure 2. (a) Transition probability along the white-dashed circle (from figure 1(b)), between $60^\circ < \theta < 210^\circ$. This angle is related to the driven frequencies as $\omega_1 = \omega_1^{(0)} + r\cos(\theta)$, and $\omega_2 = \omega_2^{(0)} + r\sin(\theta)$, where $r = 15$ MHz is the radius of the scanned spectrum. We set $\omega_1^{(0)} = \omega_2^{(0)} = 2.945$ GHz. (b) The calculated peaks demonstrate the FC in three-photon regime for the transition manifold $(4, -1)$, away from the qubit resonance frequency. Each peak represent the transition probability corresponding to a $(4, -1)$ conversion at the given frequencies. The up- and down-conversions are labeled by '+' and '−' signs on the blue and red plots, respectively. The numbers indicate the conversion magnitude, $\Omega_{1,2} = \omega_2 - \omega_1$. The full width at half maximum (FWHM) of the individual peaks are 0.36, 0.89, 0.66, 0.3, 0.2, 0.16, 0.12 MHz for the conversion magnitudes of -1.5, -1.0, -0.5, $+0.5$, $+1.0$, $+1.5$, $+2.0$ GHz, respectively.

when the inversion symmetry of the potential energy of the superconducting qubit is broken, due to longitudinal coupling.

The relaxation terms are not included for the calculations presented in this work, this approximation is valid for the system with high T1 time.

As presented in figure 1(b), the detuning of Mw1 and Mw2 from the qubit resonance frequency are $\delta_1 = 3\omega_1 - \omega_q$ and $\delta_2 = 3\omega_2 - \omega_q$, respectively. The diagram in figure 1(a) shows the case of $\delta_1 > 0$ and $\delta_2 < 0$. Since we scan a large range of detuning frequencies near and far away from the qubit resonance, $\omega_1 + \omega_2$ is not necessarily time periodic. Therefore we apply the incommensurate frequencies condition in our calculations. This requires the implementation of the *two-mode Floquet* method [21, 37]. This methodology is introduced in appendix A.

Figure 1(b) contains the calculated three-photon absorption spectrum. The number of photons involved in each transition is labeled on this contour plot. The transition probability along the white-dashed circle of radius 15 MHz, is presented in figure 2(a). The angle θ on this circle is related to the driven frequencies as $\omega_1 = \omega_1^{(0)} + r\cos(\theta)$, and $\omega_2 = \omega_2^{(0)} + r\sin(\theta)$, where $r = 15$ MHz is the radius of the scanned spectrum. We set $\omega_1^{(0)} = \omega_2^{(0)} = 2.945$ GHz. Along this circle, the first transition peak occurs near $\theta = 64.4^\circ$ where the set of the microwave frequencies is $(\omega_1, \omega_2) = (2.9511, 2.9570)$ GHz. Since $\omega_q = 8.8356$ GHz, these frequencies fulfill the three-photon transition condition when (photon number from Mw1, photon number from Mw2) $= (+6, -3)$. The *plus* and *minus* signs imply that the energy of six intake photons from Mw1 at 2.9511 GHz equals the qubit excitation energy, giving away three photons to Mw2 at 2.9570 GHz. Frequency conversion at higher photon numbers are also detectable when the two frequencies are tunned closer to the qubit resonance frequency. These higher multiphoton FC's produce the fine structure in the middle of the absorption spectrum. One can easily identify various single- and multiphoton pumping possibilities, within the three-photon transition regime, i.e. $m\omega_1 + n\omega_2 = \omega_q$ with $n + m = 3$. As we see, the FC occurs when m (or n) < 0, which implies that $|m$ (or $n)|$ number of photons is pumped from Mw1 to Mw2 (or vice-versa).

The next FC signal, in figure 2(a), is observed at $\theta = 69.7^\circ$. The set $(\omega_1, \omega_2) = (2.9498, 2.9567)$ GHz at this point corresponds to photon numbers $(5, -2)$, indicating a two-photon pumping process from Mw1 to Mw2. The next line in this spectrum is single photon pumping at $\theta = 78.2^\circ$, where $(\omega_1, \omega_2) = (2.9476, 2.9548)$ GHz. Here, three photons from Mw1 contributes to the qubit excitation, and one photon is pumped to Mw2 at 2.9548 GHz, i.e.$(4, -1)$. The transition line at $\theta = 93.5^\circ$ represents the three-photon excitation by Mw1 only, i.e. $(3, 0)$, at $\omega_1 = 2.9471$ GHz. The broad feature at $\theta = 119^\circ$ gives the contribution of two photons from Mw1 and one photon from Mw2, i.e. $(2, 1)$, at $(\omega_1, \omega_2) = (2.9368, 2.9620)$ GHz. By symmetry, the other transition peaks in this plot can be labeled properly to determine the single-and multi-photon FC's from Mw2 to Mw1 (see the labels in figures 1(b) and 2(a)).

We would like to point out that FC occurs not only for small frequency differences from the qubit transition frequency (as discussed above), but also when the microwave driving frequencies are tuned far away from the qubit transition frequency. For demonstration, the up- and down-conversions at far detuning regime are presented in figure 2(b). For each conversion case, the transition probability plot is shown in blue, and red, for up- and down-conversions, respectively. The system is driven within the $(4, -1)$ manifold, when three Mw1 photons are absorbed by the qubit and one is pumped to Mw2.

The up- and down-conversions are labeled by '+' and '−' signs on this plot, while the numbers indicate the conversion magnitude, $\Omega_{1,2} = \omega_2 - \omega_1$. Since in these calculations we keep the qubit frequency fixed, the conversion frequency is the output property that we control. For instance, in order to achieve +1 GHz up-conversion, i.e. $\Omega_{1,2} = +1$ GHz, one may tune the input frequency at $\omega_1 = 3.2785$ GHz. In this case, within the $(4, -1)$ manifold, the qubit acts as a frequency up-converter and provides the output frequency to $\omega_2 = 4.2785$ GHz. Similarly, to achieve a −1 GHz down-conversion, i.e. $\Omega_{1,2} = -1$ GHz, the Mw1 frequency is tuned to $\omega_1 = 2.6119$ GHz. Now, within the same $(4, -1)$ manifold, the qubit acts as a frequency down-converter and delivers the output frequency at $\omega_2 = 1.6119$ GHz. As presented in figure 2(b), this qubit circuit can carry out a wide range of real values for both up- and -down conversion case scenarios. The FWHM of each peak is given in the caption of figure 2(b). Each peak broadening is correlated with the difference between the lower and upper states at the avoided crossings in the quasienergy plot. This non-linearity in the dressed states picture is formulated in the denominator of equation (9) where the $4\omega_1 - \omega_2$ term appears in $E_{[4,-1,g]} = -\frac{\omega_q}{2} + 4\omega_1 - \omega_2$.

To better elucidate the photon pumping physics, we introduce an effective Hamiltonian that models each particular transition manifold. As detailed derivation in appendix B suggests, such (2×2) matrices can be extracted from the original Floquet Hamiltonian by an adiabatic elimination of the intermediate dressed states [3],

$$\hat{H}_{\mathrm{F}}^{(3,0)} = \begin{bmatrix} E_{[3,0,g]} & g_{\mathrm{eff}}^{(3,0)} \\ g_{\mathrm{eff}}^{(3,0)} & E_{[0,0,e]} \end{bmatrix}, \tag{7}$$

$$g_{\mathrm{eff}}^{(3,0)} = -\frac{4A_1^3\Delta}{E_{[3,0,g]}^3}.$$

$$\hat{H}_{\mathrm{F}}^{(2,1)} = \begin{bmatrix} E_{[2,1,g]} & g_{\mathrm{eff}}^{(2,1)} \\ g_{\mathrm{eff}}^{(2,1)} & E_{[0,0,e]} \end{bmatrix}, \tag{8}$$

$$g_{\mathrm{eff}}^{(2,1)} = -\frac{10A_1^2A_2\Delta}{E_{[2,1,g]}^3}.$$

$$\hat{H}_{\mathrm{F}}^{(4,-1)} = \begin{bmatrix} E_{[4,-1,g]} & g_{\mathrm{eff}}^{(4,-1)} \\ g_{\mathrm{eff}}^{(4,-1)} & E_{[0,0,e]} \end{bmatrix}, \tag{9}$$

$$g_{\mathrm{eff}}^{(4,-1)} = -\frac{20A_1^4A_2\Delta}{E_{[4,-1,g]}^5},$$

where $E_{[3,0,g]} = -\frac{\omega_q}{2} + 3\omega_1$, and $E_{[0,0,e]} = \frac{\omega_q}{2}$, $E_{[2,1,g]} = -\frac{\omega_q}{2} + 2\omega_1 + \omega_2$, and $E_{[4,-1,g]} = -\frac{\omega_q}{2} + 4\omega_1 - \omega_2$.

As illustrated in figure 3(a), a graph theoretic representation is helpful for understanding the multiphoton process. The three manifolds discussed in this figure are $(4, -1)$, $(3, 0)$ and $(2, 1)$. The red path in figure 3(a) indicates the $(4, -1)$ transition; the green and blue paths correspond to the $(3, 0)$ and $(2, 1)$ transitions, respectively. As can be seen in equations (7)–(9), for each case, the diagonal entries of the corresponding (2×2) Hamiltonian are the energies of the initial and final states of each graph path; and the off-diagonal coupling elements are proportional to the product of the weights of the edges

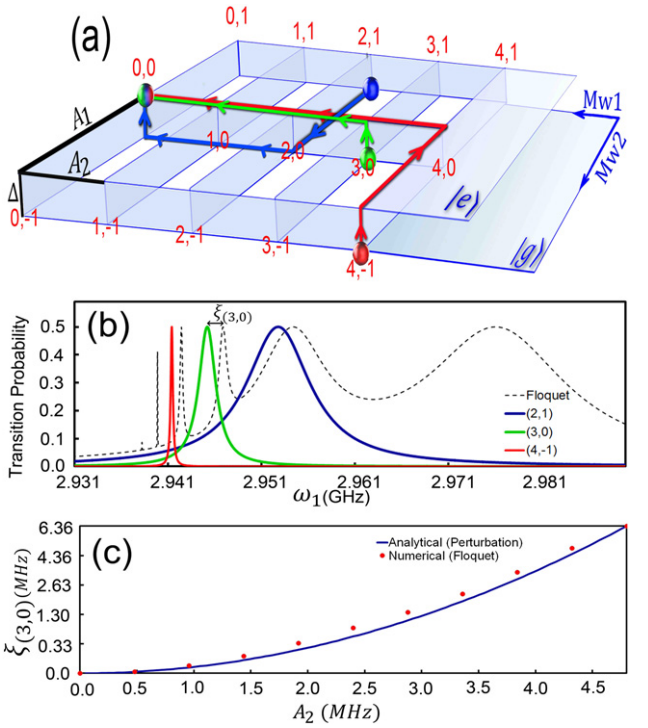

Figure 3. (a) Graph-theoretical illustration of the two-dimensional Floquet space. The three manifolds, namely $(4, -1)$, $(3, 0)$, and $(2, 1)$, are indicated as the red, green and blue paths on the graph, respectively. The parameter space of this driven system, $\{\Delta, A_1, A_2\}$, is indicated as the weights of the graph edges. The transition spectrum corresponding to these paths, obtained from equations (7)–(9), are presented in (b). The full-Floquet result is given as black-dashed line for comparison purpose. (c) Comparison of the Floquet and analytical, equation (10), values for the shift observed in the $(3, 0)$ peak position as a function of (A_2). The Mw1 power is kept constant at $A_1 = 0.8$ GHz. The $(3, 0)$ peak is originally expected to be seen at $\omega_q/3 = 2.9452$ GHz (i.e. when $A_2 = 0$).

involved in each path. These weights construct the parameter space of the driven system, $\{\Delta, A_1, A_2\}$. The transition probabilities presented in figure 3(b) are obtained by solving the eigenvalue problem in equations (7)–(9). The prominent peaks in the full Floquet spectrum are reproduced, but shifted, with the reduced graph-theoretic Hamiltonian approach. The spectral peaks deviate from the bare states due to photon dressing [38]. Within the rotating-wave approximation, such resonance shift can be expressed analytically in the form [21, 37],

$$\xi_N = \frac{A_1^2}{2(\omega_1 - \omega_2)}\left(\frac{1}{N} + \frac{(A_1/A_2)^2}{N+1}\right), \tag{10}$$

where N indicates the number of photons involved in the transition, $N = n + m$. This effect is presented in figure 3(c) for the shift observed in the position of the $(3, 0)$ transition peak.

For each manifold, the peak broadening can be explained quantitatively within the provided effective Hamiltonian approximation, equations (7)–(9). The width of the peaks, can be determined by the frequency-dependent effective coupling strengths, g_{eff}. The FWHM of the individual peaks in figure 3(b) are 8.3 MHz, 2.2 MHz, and 0.27 MHz for $(2, 1)$,

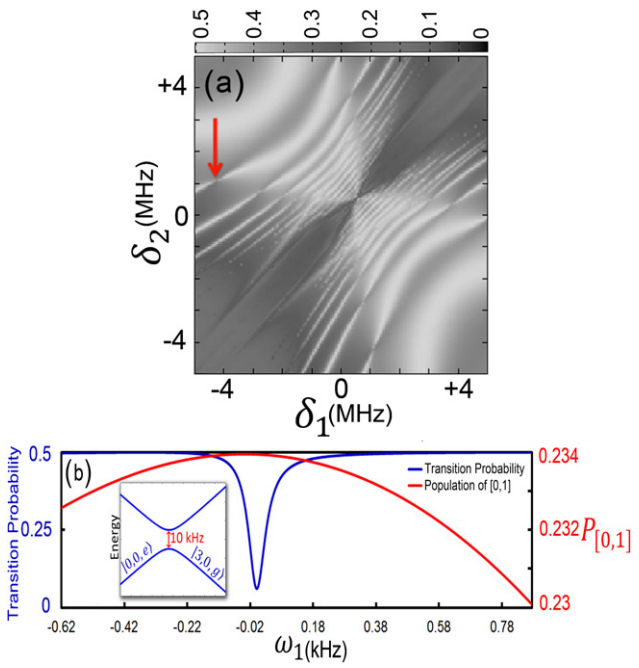

Figure 4. (a) The closer view of the central region of the interference patterns from the calculated absorption spectrum. Frequency detuning step size is 40 kHz. The arrow indicates the position of the three-photon suppression in the $(n_1 = 0, n_2 = 3)$ manifold, where $n_{1,2}$ are the number of photons absorbed or emitted in the two microwaves. (b) Three-photon transition suppression (solid blue line) within a small range of frequency tunning. The population trapping in the $|0, 1, g >$ state is given as the solid red line. This result is obtained from the reduced Floquet matrix calculations, when only up to three-photon absorption and emission processes are allowed for each microwave modes. The Mw1 frequency on x-axis is reported as the detuning around the suppression point, $(\omega_1^{\rm sup} = 2.9456$ GHz). For the results in (b) we set the peak intensities of the microwaves as $A_1 = 0.24$ MHz, and $A_2 = 0.024$ MHz. The black and white map in (a) shows the transition probability from $|g\rangle$ to $|e\rangle$. The inset in (b) shows the anti-crossing in the eigenenergy spectrum at the suppression point. The energy gap of $\Delta_g = 10$ kHz gives a trapping time $2\pi/\Delta_g \sim 100$ μs.

$(3, 0)$ and $(4, -1)$ peaks, respectively, which is in accordance with the following hierarchy, $g_{\rm eff}^{(2,1)} > g_{\rm eff}^{(3,0)} > g_{\rm eff}^{(4,-1)}$.

Another interesting feature in the presented absorption spectrum is the appearance of transition suppressions at specific frequencies. We address the origin of this effect in figure 4. The arrow in figure 4(a) indicates the transition suppression in the (0, 3) manifold. The effect is also observed in the other three-photon manifolds, e.g. $(-1, 4), (-2, 5), (-3, 6)$, etc. The transmission blockade of more than two photons has been previously reported [39, 40]. The suppression of the transition probability can also be due to the coherent superposition of high-order Fourier harmonics closing the dynamical gap between the Floquet states [41].

To explain the mechanism of such suppression for the $(0, 3)$ manifold, we reduced the size of the original Floquet matrix, equation (A10), by allowing only the absorption and emission processes up to three photons for each microwave mode. The Fourier index set for each mode is now reduced to $m_i = 0, \pm1, \pm2, \pm3$. The bare state is denoted by index 0, and the dresses states are given by photon number $\pm1, \pm2, \pm3$. The truncated matrix has now the size of $2 \times 7 \times 7 = 98$. Since we have removed all of the higher multiphoton contributions from the Floquet matrix, the only available paths on the reduced two-dimensional Floquet space involve only four states, see figure B1.

As presented in the inset in figure 4(b), the suppression effect can be achieved by tuning the driving frequencies in the vicinity of a crossing between the Floquet states. The three-photon resonance suppression can be explained by population trapping on the graph vertices connecting the $|0, 3, g >$ state to the $|0, 0, e >$ state. As the solid red curve in figure 4(b) indicates, such population trapping occurs in the $|0, 1, g >$ state. The occurrence of a maximum in the $|0, 1, g >$ population manifests itself as the suppression of the (0, 3) transition probability (solid blue line). This suppression and population trapping occurs at the point of closest avoided crossing between the two states, which gives the trapping time of $2\pi/\Delta_g \sim 100$ μs $\gg T_1$.

In this work, nonlinear multiphoton up/down frequency conversion in a superconducting flux circuit is demonstrated with a full Floquet technique. Multiphoton spectra over a wide microwave range, show photon pumping from one microwave field to another. To reveal the underlying physics in the single- and multiphoton pumping mechanisms, effective Hamiltonians are derived with a graph-theoretic approach, to model the transitions. The suppression of pumping at particular resonant frequencies are shown to be due to coherent population trapping in dressed states of the qubit, due to sharp avoided crossing between qubit states, much the same as the Mach–Zander interfrometry was proposed with superconducting qubits [32]. Further work will attempt to include the relaxation channels, and the effect of the higher states on the absorption spectrum and the frequency conversion scheme. Implementation of the proposed scheme with on-chip microwave transmission line resonators may provide a way to measure the quantum efficiency of the prospective circuit quantum electrodynamics designs. The proposed design and theoretical approach maybe of interest in quantum transducer design and fabrication for future quantum networks, and to maintain the inter-connectivity of remote superconducting quantum machines.

Acknowledgments

HZJ acknowledge the NSF support through a Grant for ITAMP at Harvard University. SH is supported in part by NSF (PHY-1314861). This work was partially supported by the NKRDP of China (Grant No. 2016YFA0301801), NSFC (11474154), PAPD, and Dengfeng Project B of Nanjing University.

Appendix A. Two-mode Floquet formalism

In our theoretical formalism, we consider the interaction of the qubit (modeled as a two-level system) with two microwaves, equations (4)–(6). The relaxation terms have not been included in the interaction Hamiltonian. At high T1 values, this approximation does not affect the observation of the multiphoton

pumping qualitatively. The assignment of Mw1 and Mw2 for the two microwave fields are arbitrary. Within the two-mode semiclassical Floquet approach the system will be treated quantum mechanically whereas the fields classically. The time evolution of the wave function is determined by the time-dependent Schrödinger equations (in atomic units, $\hbar = m_e = e = 1$),

$$i\frac{\partial\psi}{\partial t} = \hat{H}\psi. \tag{A1}$$

According to the generalized Floquet theory, The Hamiltonian of the driven two-level system, with bare eigenstates ($|g>, |e>$) and eigenvalues (E_g, E_e), has a solution that can be written as

$$\Psi(t) = \exp(-iqt)\phi(t), \tag{A2}$$

where $\Phi(t)$ is periodic in time and q is called the quasienergy. Substituting equation (A2) into equation (A1), we obtain an eigenvalue equation for the quasienergy,

$$\left[\hat{H}(t) - i\frac{\partial}{\partial t}\right]\Phi(t) = q\Phi(t). \tag{A3}$$

Since we are scanning a wide range of the two microwave frequencies, we consider the case of incommensurate frequencies, where the combined ω_1 and ω_2 frequencies is not necessarily periodic in time. According to the many-mode Floquet theorem, one can transfer this time-dependent problem into an equivalent time-independent infinite dimensional Floquet matrix eigenvalue problem, so that the temporal part of the Hamiltonian $H(t)$ and the quasienergy eigenfunction $\Phi(t)$ can be expanded with the double-Fourier components of any arbitrary set of the fundamental frequencies (ω_1, ω_2),

$$\Phi(t) = \sum_{m_1,m_2} \Phi^{[m_1,m_2]} \exp[-i(m_1\omega_1 t + m_2\omega_2 t)], \tag{A4}$$

$$\hat{H}(t) = \sum_{m_1,m_2} H^{[m_1,m_2]} \exp[-i(m_1\omega_1 t + m_2\omega_2 t)], \tag{A5}$$

where the time-independent coefficients $\Phi^{[m_1,m_2]}$ and $H^{[m_1,m_2]}$ are spanned by any orthonormal basis set. We employ the Floquet-state nomenclature,

$$|\alpha, \{m_1, m_2\}> \cong |\alpha> \otimes |\{m_1, m_2\}>, \quad \alpha = g, e \tag{A6}$$

where g and e are system indices, representing the ground and excited states of the two-level system, respectively. m_1 and m_2 are the Fourier indices that run from $-\infty$ to $+\infty$. Substituting equation (A4), (A5) into equation (A3) and employing equation (A6), gives the following time-independent two-mode Floquet matrix eigenvalue equation,

$$\sum_e \sum_{\{k\}} < g; \{m_1, m_2\}|\hat{H}_{\rm F}|e; \{k\} >< e; \{k\}|q_{\mu;\{n\}} >$$
$$= q_{\mu;\{n\}} < g; \{m_1, m_2\}|q_{\mu;\{n\}} >, \tag{A7}$$

where $q_{\mu\nu}$ is the quasienergy eigenvalue and $|q_{\mu\nu}>$ is the corresponding eigenvector. The time-independent two-mode Floquet matrix, $\hat{H}_{\rm F}$, is defined in terms of equation (A6). More explicitly, $\hat{H}_{\rm F}$ can be written, in matrix form as,

$$< g; \{m_i\}|\hat{H}_{\rm F}|e; \{k\} >$$
$$= \hat{H}_{ge}^{[m-k]} + \sum_i m_i\omega_i\delta_{ge}\delta_{\{m_i\};\{k\}}, \quad i = 1, 2 \tag{A8}$$

where $\delta_{\{i,j\}}$ is the Kronecker delta function. For the effective Hamiltonian of the superconducting flux qubit,

$$\hat{H} = -\frac{1}{2}\begin{bmatrix} \varepsilon_0 + \mathcal{E}(t) & \Delta \\ \Delta & -\varepsilon_0 + \mathcal{E}(t) \end{bmatrix}, \tag{A9}$$

the structure of the Floquet matrix, which is Hermitian, is illustrated below (assuming $\omega_q \simeq \varepsilon_0$),

$$\hat{H}_{\rm F} = \begin{bmatrix} \ddots & & & & & \\ & A - 2\omega_2 I & B & 0 & 0 & 0 \\ & B & A - \omega_2 I & B & 0 & 0 \\ & 0 & B & A & B & 0 \\ & 0 & 0 & B & A + \omega_2 I & B \\ & 0 & 0 & 0 & B & A + 2\omega_2 I \\ & & & & & \ddots \end{bmatrix}, \tag{A10}$$

where,

$$A = \begin{bmatrix} \ddots & & & & & \\ & C - 2\omega_1 I & X & 0 & 0 & 0 \\ & X & C - \omega_1 I & X & 0 & 0 \\ & 0 & X & C & X & 0 \\ & 0 & 0 & X & C + \omega_1 I & X \\ & 0 & 0 & 0 & X & C + 2\omega_1 I \\ & & & & & \ddots \end{bmatrix}, \tag{A11}$$

$$B = \begin{bmatrix} Y & 0 & 0 & 0 & 0 \\ 0 & Y & 0 & 0 & 0 \\ 0 & 0 & Y & 0 & 0 \\ 0 & 0 & 0 & Y & 0 \\ 0 & 0 & 0 & 0 & Y \end{bmatrix}, \tag{A12}$$

$$C = -\frac{1}{2}\begin{bmatrix} \omega_q & \Delta \\ \Delta & -\omega_q \end{bmatrix}, \tag{A13}$$

$$X = -\frac{1}{4}\begin{bmatrix} A_1 & 0 \\ 0 & -A_1 \end{bmatrix}, \tag{A14}$$

$$Y = -\frac{1}{4}\begin{bmatrix} A_2 & 0 \\ 0 & -A_2 \end{bmatrix}. \tag{A15}$$

The multiply periodic structure of $H_{\rm F}$ holds the following important periodic relationships for its eigenvalues, and eigenvectors,

$$q_{\mu;\{n+k\}} = q_{\mu;\{n\}} + \sum_i k_i\omega_i, \quad i = 1, 2 \tag{A16}$$

and

$$< g; \{m_i + k\}|q_{\mu;\{n+k\}} >=< g; \{m_i\}|q_{\mu;\{n\}} > . \quad \text{(A17)}$$

Eigenvalues of the Floquet matrix in equation (A10) are numerically solved by truncating the number of Floquet blocks. The converged results presented in this paper are generated by the inclusion of 21 blocks (adsorption and emission up to 10 photons for each mode). After solving the eigenvalue problem of the Floquet matrix, the time-averaged transition probability between $|g>$ and $|e>$ can be computed as,

$$\overline{P}_{g\to e} = \sum_{\mu}\sum_{\{n\}}\sum_{\{m\}} | < e; \{m\}|q_{\mu;\{n\}} > . < q_{\mu;\{n\}}|g; \{0\} > |^2. \quad \text{(A18)}$$

Extending Shirley's expression, [42], for the case of a two-level system in a monochromatic field, equation equation (A18) can be cast into an alternative form,

$$\overline{P}_{g\to e} = \frac{1}{2}\left[1 - 4\left(\frac{\partial q_{g00}}{\partial \omega_q}\right)^2\right], \quad \text{(A19)}$$

which shows that $\overline{P}_{g\to e} \leqslant \frac{1}{2}$.

Equation (A18) is corresponding to the probability of finding the qubit system in the excited state in the experiment. The transition probability plots presented in this work are obtained by applying this equation. There has been no approximation made in equation (A18) to solve the time-dependent Hamiltonian of equation (4). Therefore this matrix can be applied for all parameter regimes. Indeed, all the theoretical results presented in figures 1(b) and 4(a) are obtained by solving the eigenvalue problem of this two-mode Floquet matrix, and calculating the time-averaged transition probabilities between $|g>$ and $|e>$ using equation (A18).

The effects of the microwave amplitudes and the tunnel splitting on the transition spectrum are evaluated in figure A1. Besides the broadening effect, the shift in the position of the $(0, 3)$ line is also indicated by a black arrow to demonstrate the pronounced effect of increasing the tunnel splitting in figure A1(b), compared to the Stark shift in figure A1(a).

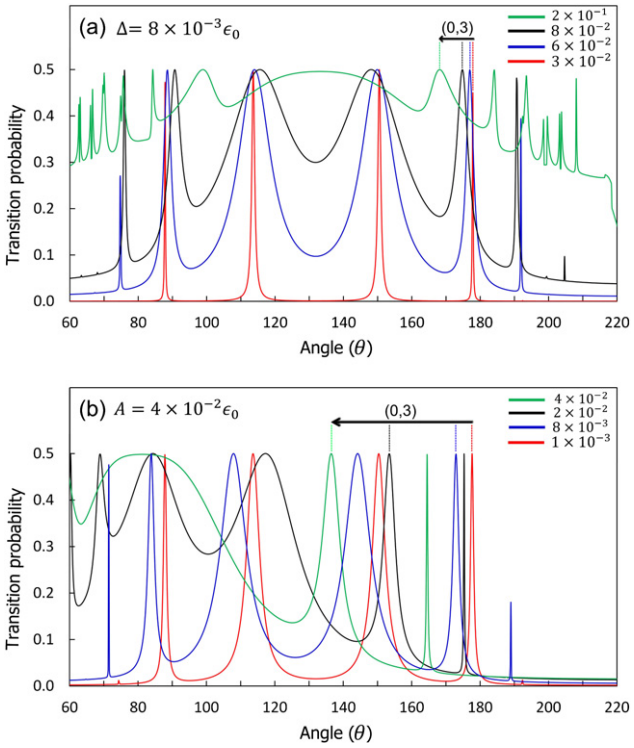

Figure A1. (a) The effect of the microwave peak intensity, A/ε_0, on the transition probability along the white dashed line in figure 1(b). Here, the tunnel splitting is kept constant at $\Delta = 8 \times 10^{-3}\varepsilon_0$. (b) The effect of the tunnel splitting, Δ/ε_0, is considered at constant microwave peak intensity $A = 4 \times 10^{-2}\varepsilon_0$. For these calculations we set $A = A_1 = A_2$. Besides the broadening effect, the shift in the position of the $(0, 3)$ line is also indicated by a black arrow to demonstrate the pronounced effect of increasing the tunnel splitting in (b), compared to the Stark shift in (a).

Appendix B. Effective Hamiltonian in multiphoton region

Although truncated, the size of the Floquet matrix, equation (A10), that one needs to solve to get each data points in a contour plot, like the one presented in figure 1(b), can increase dramatically for the higher-order processes. In this study, to obtain convergence in the three-photon transition regime, we truncated the matrix at $2 \times 21 \times 21 = 882$, which includes all the transition channels for the qubit with ± 10 photons processes. Here, we introduce an effective Hamiltonian approach that models each particular transition manifold. We show that such (2×2) matrices can be extracted from the original Floquet Hamiltonian, equation (A10) and reproduce the main features of the solution of the full Floquet matrix.

Figure B2 shows the four possible paths from $|3, 0, g>$ to $|0, 0, e>$, which are responsible for the $(3, 0)$ peak reported in figure 1(b). The truncated Floquet Hamiltonian for this manifold can be written as,

$$\hat{H}_F = \begin{bmatrix} -\frac{\omega_q}{2} + 3\omega_1 & \Delta & 0 & 0 & 0 \\ \Delta & \frac{\omega_q}{2} + 3\omega_1 & A_1 & 0 & 0 \\ 0 & A_1 & \frac{\omega_q}{2} + 2\omega_1 & A_1 & 0 \\ 0 & 0 & A_1 & \frac{\omega_q}{2} + \omega_1 & A_1 \\ 0 & 0 & 0 & A_1 & \frac{\omega_q}{2} \end{bmatrix}. \quad \text{(B1)}$$

For any of these paths, one can write the set of five Schrödinger equations for the evolution of the dressed states involved, with their corresponding amplitudes, $(c_1 - c_5)$. For instance, the path presented in the top-left panel in figure B2, would be formulated as,

$$\begin{aligned} i\dot{c}_1 &= (-\frac{\omega_q}{2} + 3\omega_1)c_1 + \Delta c_2, \\ i\dot{c}_2 &= (\frac{\omega_q}{2} + 3\omega_1)c_2 + A_1 c_3, \\ i\dot{c}_3 &= (\frac{\omega_q}{2} + 2\omega_1)c_3 + A_1 c_4, \\ i\dot{c}_4 &= (\frac{\omega_q}{2} + \omega_1)c_4 + A_1 c_5, \\ i\dot{c}_5 &= (\frac{\omega_q}{2})c_5. \end{aligned} \quad \text{(B2)}$$

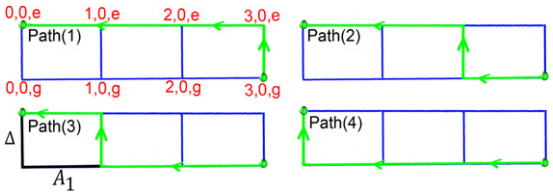

Figure B1. Graph-theoretical illustration of the fours possible paths on the one-dimensional Floquet subspace, representing the $(3, 0)$ transition manifold. The weight of all the horizontal edges is the peak amplitude of Mw1, A_1. The weight of all the vertical edges is the tunnel splitting, Δ.

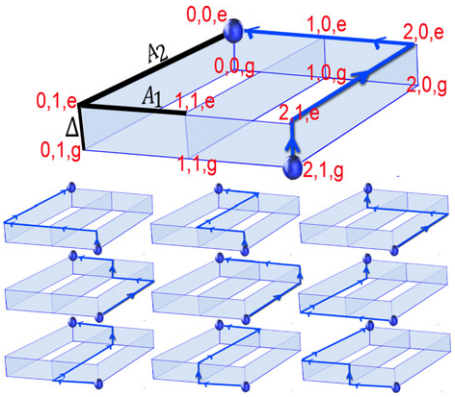

Figure B2. Graph-theoretical illustration of the ten possible paths on the two-dimensional Floquet subspace, representing the $(2, 1)$ transition manifold. The weight of the edges are given as the Mw1 power, A_1, Mw2 power, A_2, and the tunnel splitting, Δ.

Under adiabatic approximation, we can assume that the population of the three intermediate states, do not change significantly, i.e. $\dot{c}_2 = \dot{c}_3 = \dot{c}_4 = 0$. This gives,

$$\begin{aligned} c_2 &= -\frac{A_1 c_3}{\frac{\omega_q}{2} + 3\omega_1}, \\ c_3 &= -\frac{A_1 c_4}{\frac{\omega_q}{2} + 2\omega_1}, \\ c_4 &= -\frac{A_1 c_5}{\frac{\omega_q}{2} + \omega_1}. \end{aligned} \tag{B3}$$

The effective coupling rate between the initial,$|3, 0, g>$ and final, $|0, 0, e>$, states, through this particular path, can be then obtained by plugging in these coefficients into the c_1 and c_5 rate equations in equation (B2),

$$g_{\text{eff}}^{\text{path}(1)} = -\frac{A_1^3 \Delta}{E_{[3,0,e]} E_{[2,0,e]} E_{[1,0,e]}}, \tag{B4}$$

where $E_{[3,0,e]} = \frac{\omega_q}{2} + 3\omega_1$, $E_{[2,0,e]} = \frac{\omega_q}{2} + 2\omega_1$, and $E_{[1,0,e]} = \frac{\omega_q}{2} + \omega_1$. To obtain the total effective coupling rate, one should sum over the coupling strengths through other three possible pathways; meaning that,

$$g_{\text{eff}}^{\text{total}} = g_{\text{eff}}^{\text{path}(1)} + g_{\text{eff}}^{\text{path}(2)} + g_{\text{eff}}^{\text{path}(3)} + g_{\text{eff}}^{\text{path}(4)}, \tag{B5}$$

where,

$$\begin{aligned} g_{\text{eff}}^{\text{path}(2)} &= -\frac{A_1^3 \Delta}{E_{[2,0,g]} E_{[2,0,e]} E_{[1,0,e]}}, \\ g_{\text{eff}}^{\text{path}(3)} &= -\frac{A_1^3 \Delta}{E_{[2,0,g]} E_{[1,0,g]} E_{[1,0,e]}}, \\ g_{\text{eff}}^{\text{path}(2)} &= -\frac{A_1^3 \Delta}{E_{[2,0,g]} E_{[1,0,g]} E_{[0,0,g]}}. \end{aligned} \tag{B6}$$

with $E_{[2,0,g]} = -\frac{\omega_q}{2} + 2\omega_1$, $E_{[1,0,g]} = -\frac{\omega_q}{2} + \omega_1$, and $E_{[0,0,g]} = -\frac{\omega_q}{2}$.

Equation (B6) can be simplified by writing all the energies in terms of $E_{[3,0,g]}$ as (see figure B2)

$$\begin{aligned} E_{[3,0,e]} &= E_{[3,0,g]} + \Delta, \\ E_{[2,0,e]} &= E_{[3,0,g]} + \Delta - A_1, \\ E_{[1,0,e]} &= E_{[3,0,g]} + \Delta - 2A_1, \\ E_{[2,0,g]} &= E_{[3,0,g]} - A_1, \\ E_{[1,0,g]} &= E_{[3,0,g]} - 2A_1. \end{aligned} \tag{B7}$$

By doing some algebra and keeping only the leading terms in $E_{[3,0,g]}$, the (2×2) effective Hamiltonian can be approximated as,

$$\hat{H}_{\text{F}}^{(3,0)} = \begin{bmatrix} E_{[3,0,g]} & g_{\text{eff}}^{(3,0)} \\ g_{\text{eff}}^{(3,0)} & E_{[0,0,e]} \end{bmatrix}, \quad g_{\text{eff}}^{(3,0)} = -\frac{4A_1^3 \Delta}{E_{[3,0,g]}^3}, \tag{B8}$$

where $E_{[3,0,g]} = -\frac{\omega_q}{2} + 3\omega_1$, and $E_{[0,0,e]} = \frac{\omega_q}{2}$. It is worth noting that in equations (B4)–(B6) all the four paths share the same nominator, which remains the same in equation (B8).

The same approach can be used to obtain the (2×2) effective Hamiltonian for the $(2, 1)$ transition manifold. As can be seen in figure B1, there are ten possible paths that connect the $|2, 1, g>$ vertex to $|0, 0, e>$ vertex. The only task here would be to count for the weighted edges for one of these paths. It should be mentioned again that the nominator of the effective coupling in all these ten paths are the same as it appears in equation (B9). Within the same approximation discussed above, one could simply write,

$$\hat{H}_{\text{F}}^{(2,1)} = \begin{bmatrix} E_{[2,1,g]} & g_{\text{eff}}^{(2,1)} \\ g_{\text{eff}}^{(2,1)} & E_{[0,0,e]} \end{bmatrix}, \quad g_{\text{eff}}^{(2,1)} = -\frac{10A_1^2 A_2 \Delta}{E_{[2,1,g]}^3} \tag{B9}$$

where $E_{[2,1,g]} = -\frac{\omega_q}{2} + 2\omega_1 + \omega_2$.

The (2×2) effective Hamiltonian for $(4, -1)$ is obtained similarly, considering the fact that there will be 20 possible pathways connecting $E_{[4,-1,g]}$ and $E_{[0,0,e]}$.

$$\hat{H}_{\text{F}}^{(4,-1)} = \begin{bmatrix} E_{[4,-1,g]} & g_{\text{eff}}^{(4,-1)} \\ g_{\text{eff}}^{(4,-1)} & E_{[0,0,e]} \end{bmatrix}, \quad g_{\text{eff}}^{(4,-1)} = -\frac{20A_1^4 A_2 \Delta}{E_{[4,-1,g]}^5}, \tag{B10}$$

where $E_{[4,-1,g]} = -\frac{\omega_q}{2} + 4\omega_1 - \omega_2$.

ORCID iDs

H Z Jooya https://orcid.org/0000-0003-1636-7539
G Sun https://orcid.org/0000-0002-7847-3460

References

[1] Neill C *et al* 2018 *Science* **360** 195
[2] Buluta I, Ashhab S and Nori F 2011 *Rep. Prog. Phys.* **74** 104401
[3] Kockum A F, Macra V, Garziano L, Savasta S and Nori F 2017 *Sci. Rep.* **7** 5313
[4] Martin I, Refael G and Halperin B 2017 *Phys. Rev.* X **7** 041008
[5] Abdo B, Sliwa K, Schackert F, Bergeal N, Hatridge M, Frunzio L, Stone A D and Devoret M 2013 *Phys. Rev. Lett.* **110** 173902
[6] Zhang M, Zou C-L and Jiang L 2018 *Phys. Rev. Lett.* **120** 020502
[7] Xiang Z-L, Ashhab S, You J Q and Nori F 2013 *Rev. Mod. Phys.* **85** 623
[8] Inomata K, Koshino K, Lin Z R, Oliver W D, Tsai J S, Nakamura Y and Yamamoto T 2014 *Phys. Rev. Lett.* **113** 063604
[9] Moon K and Girvin S M 2005 *Phys. Rev. Lett.* **95** 140504
[10] Deppe F *et al* 2008 *Nat. Phys.* **4** 686
[11] Yoshihara F, Fuse T, Ashhab S, Kakuyanagi K, Saito S and Semba K 2017 *Nat. Phys.* **13** 44
[12] Kennes D M, de la Torre A, Ron A, Hsieh D and Millis A J 2018 *Phys. Rev. Lett.* **120** 127601
[13] Hensinger W K 2011 *Nature* **476** 155
[14] Friedman J R, Patel V, Chen W, Tolpygo S K and Lukens J E 2000 *Nature* **406** 43
[15] van der Wal C H, ter Haar A C J, Wilhelm F K, Schouten R N, Harmans C J P M, Orlando T P, Lloyd S and Mooij J E 2000 *Science* **290** 773
[16] Shevchenko S N, Omelyanchouk A N and Ilâichev E 2012 *Low Temp. Phys.* **38** 283
[17] Felicetti S, Rossatto D Z, Rico E, Solano E and Forn-Díaz P 2018 *Phys. Rev.* A **97** 013851
[18] Malekakhlagh M and Rodriguez A W 2019 *Phys. Rev. Lett.* **122** 043601
[19] Wallraff A, Duty T, Lukashenko A and Ustinov A V 2003 *Phys. Rev. Lett.* **90** 037003
[20] Saito S, Thorwart M, Tanaka H, Ueda M, Nakano H, Semba K and Takayanagi H 2004 *Phys. Rev. Lett.* **93** 037001
[21] Chu S-I and Telnov D A 2004 *Phys. Rep.* **390** 1
[22] Oelsner G, Macha P, Astafiev O V, Il'ichev E, Grajcar M, Hübner U, Ivanov B I, Neilinger P and Meyer H-G 2013 *Phys. Rev. Lett.* **110** 053602
[23] Greenberg Y S 2007 *Phys. Rev.* B **76** 104520
[24] Jooya H Z, Reihani K and Chu S-I 2016 *Sci. Rep.* **6** 174518
[25] Sun G, Wen X, Mao B, Yu Y, Chen J, Xu W, Kang L, Wu P and Han S 2011 *Phys. Rev.* B **83** 180507
[26] Wilson C M, Duty T, Persson F, Sandberg M, Johansson G and Delsing P 2007 *Phys. Rev. Lett.* **98** 257003
[27] Fink J M, Bianchetti R, Baur M, Göppl M, Steffen L, Filipp S, Leek P J, Blais A and Wallraff A 2009 *Phys. Rev. Lett.* **103** 083601
[28] Pan J, Jooya H Z, Sun G, Fan Y, Wu P, Telnov D A, Chu S-I and Han S 2017 *Phys. Rev.* B **96** 174518
[29] Han S, Lapointe J and Lukens J E 1989 *Phys. Rev. Lett.* **63** 1712
[30] Chiorescu I, Nakamura Y, Harmans C J P M and Mooij J E 2003 *Science* **299** 1869
[31] Leggett A J, Chakravarty S, Dorsey A T, Fisher M P A, Garg A and Zwerger W 1987 *Rev. Mod. Phys.* **59** 1
[32] Oliver W D, Yu Y, Lee J C, Berggren K K, Levitov L S and Orlando T P 2005 *Science* **310** 1653
[33] Son S-K, Han S and Chu S-I 2009 *Phys. Rev.* A **79** 032301
[34] Zhao Y-J, Liu Y-L, Liu Y-x. and Nori F 2015 *Phys. Rev.* A **91** 053820
[35] Liu Y-x, You J Q, Wei L F, Sun C P and Nori F 2005 *Phys. Rev. Lett.* **95** 087001
[36] Liu Y-X, Yang C-X, Sun H-C and Wang X-B 2014 *New J. Phys.* **16** 015031
[37] Ho T-S, Chu S-I and Tietz J V 1983 *Chem. Phys. Lett.* **96** 464
[38] Ahmad F and Bullough R K 1974 *J. Phys. B: At. Mol. Phys.* **7** L275
[39] Miranowicz A, Paprzycka M, Liu Y-X, Bajer J C V and Nori F 2013 *Phys. Rev.* A **87** 023809
[40] Garziano L, Macrì V, Stassi R, Di Stefano O, Nori F and Savasta S 2016 *Phys. Rev. Lett.* **117** 043601
[41] Gagnon D, Fillion-Gourdeau F M C, Dumont J, Lefebvre C and MacLean S 2017 *Phys. Rev. Lett.* **119** 053203
[42] Shirley J H 1965 *Phys. Rev.* **138** B979